Chitosan as a Water-Developable 193 nm Photoresist for Green Photolithography

Olha Sysova, Paule Durin, Corinne Gablin, Didier Léonard, Alexandre Téolis, Stéphane Trombotto, Thierry Delair, Dominique Berling, Isabelle Servin, Raluca Tiron, et al.

Chitosan as water developable 193 nm photoresist for green photolithography

Olha Sysova[1,2], Paule Durin[3,4], Corinne Gablin[4], Didier Léonard[4], Alexandre Téolis[6], Stéphane Trombotto[6], Thierry Delair[6], Dominique Berling[1,2], Isabelle Servin[5], Raluca Tiron[5], Arnaud Bazin[5], Jean-Louis Leclercq[3], Yann Chevolot[3], Olivier Soppera[1,2,*]

[1] *Université de Haute-Alsace, CNRS, IS2M UMR 7361, F-68100 Mulhouse, France*

[2] *Université de Strasbourg, France*

[3] *Univ Lyon, CNRS, INSA Lyon, Ecole Centrale de Lyon, Université Claude Bernard Lyon 1, CPE Lyon, INL, UMR5270, 69134 Ecully Cedex, France*

[4] *Univ Lyon, CNRS, Université Claude Bernard Lyon 1, Institut des Sciences Analytiques, UMR 5280, 5, rue de la Doua, F-69100 Villeurbanne, France.*

[5] *Univ. Grenoble Alpes, CEA, LETI, F-38000 Grenoble, France*

[6] *Univ Lyon, CNRS, UMR 5223, Ingénierie des Matériaux Polymères, Université Claude Bernard Lyon 1, INSA Lyon, Université Jean Monnet, F-69622 VILLEURBANNE Cédex, France*

[*] contact : olivier.soppera@uha.fr

Keywords

Photolithography, chitosan, photoresist, Deep-UV, biosourced materials

Abstract

The development of environmentally friendly materials and processes is a major issue that concerns all industrial sectors, including microelectronics. The aim of this study is to demonstrate the possibility of using chitosan-based photoresists for microelectronic applications on silicon by 193 nm photolithography. The photopatterning of chitosan films is demonstrated and analyzed by different spectroscopy and microscopy techniques. In particular, it is shown that 193 nm irradiation allows to induce chain breaks that modify the solubility of chitosan in the aqueous developing solution, without denaturing the chitosan macromolecule chains. This mechanism allows to obtain patterns and it is shown that these patterns can be

transferred by physical etching into silica. It is also demonstrated that the formulated resins are compatible with industrial spin-coating and exposure tools, which opens very interesting perspectives for these chitosan-based positive resins in a microelectronic context.

1. Introduction

Photolithography is a key-step in micro and nanofabrication in the world of microelectronics. Among different photolithography techniques, Deep-UV lithography (DUV) remains the most used technology in the industry, as it allows one to obtain high-resolution patterns in a relatively short time. However, one of the significant disadvantages of photolithography is the use of toxic resists and solvents, as well as the process of their development, which usually requires harmful developing solutions like tetramethyl ammonium hydroxide (TMAH). [1,2,3] Thus, the future is to find more ecologically friendly components that will come from biosourced materials and be potentially biodegradable. Different types of patterning of biosourced materials have been proposed in the literature, covering the different technologies used for micro and nanopatterning, extreme UV lithography (EUV), [4] electron beam lithography (E-beam) [5,6,7] or nanoimprint [8] that are used to obtain patterns with different resolution capacities.

Gelatin, silk protein and egg albumin are the most common examples of protein-based photoresists. In [9,10] authors reported the potential application of silk fibroin as a resist for 2D and 3D E-beam writing achieving sub-15 nm resolution. Gelatin-based hydrogel was patterned by 2-photon polymerization lithography [11] to obtain 3D microstructures. However, the resulting patterned structures were mainly destined to be used for the pharmaceutical or biological purposes and not for microelectronic applications. As for the egg white albumin, features above 5 μm were obtained after etching [7] followed by a long development step, which can be hardly applicable to the technological process. It is also preferable to use waste or recycled material, and not a product used in the food industry.

Among other biosourced materials, chitosan [12] and cellulose-based [8] resists were reported to be used for nanoimprint lithography obtaining submicrometric features. Nevertheless, the biggest disadvantage of the nanoimprint is the potential pattern defectivity which comes from the direct contact of the mold and resist. [13]

Close attention has been also paid to polysaccharides that could be good candidate for commercial photoresist replacement. It was shown that cellulose [4,8] alginate [14], dextrin [6], pullulan [15] can be used as a photolithography resist. Nevertheless, the above-mentioned

polysaccharides need to be chemically modified to acquire electro- or photosensitivity. In this case, adding acryloyl or epoxy groups is outside the scope of a green resist.

It was shown recently that chitosan and chitosan salts can be used without chemical modification as a positive resist for 248nm or E-Beam lithography. [16,17,18] In this paper, we show that we can achieve photopatterning of raw chitosan at 193 nm and that patterned chitosan is suitable for dry etching for pattern transfer into silica by dry etching. In this frame, chitosan appears thus as an ideal candidate for replacing commercial synthetic resists, since it does not need additional modifications, and development of patterns can be achieved with water or a slightly acidified solution after 193 nm irradiation. The photoinduced physico-chemical modification of the chitosan thin film by 193 nm exposure is characterized to understand the mechanism of photopatterning and therefore to control this critical technological step in micro-device fabrication chain (yield, throughput, critical dimensions…). This study includes the demonstration of photopatterning at 193 nm, the study of photo-induced phenomena explaining this behavior. We show the possibility of using this material in an industrial microelectronic context thanks to deposition and exposure on industrial instruments. Preliminary etching tests prove the compatibility of this photoresist with such facilities (**Figure 1**).

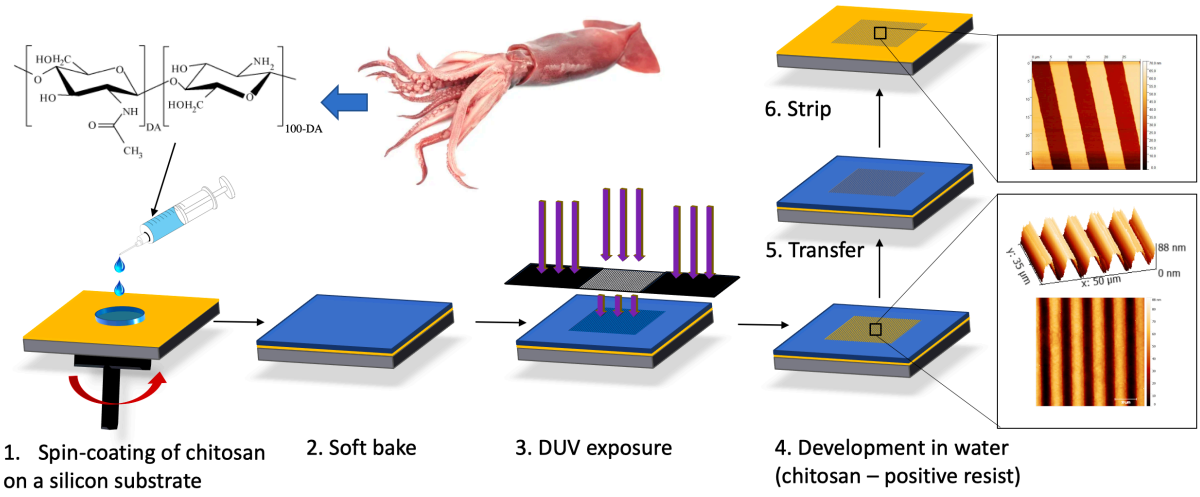

Figure 1. Schematic view of the procedure for using chitosan as a positive-tone resist for DUV lithography. (1) First step is to spin-coat an aqueous solution of chitosan onto the silicon substrate. (2) This step is followed by a soft bake at 150°C for 5 minutes. (3) The film is then exposed to DUV radiation via a binary chrome mask, which leads to molecule scissoring and decrease of molar mass in the exposed zones. (4) To reveal the patterns on the film surface, deionized water is used. Thus, the solubility of the film in the irradiated zones increases and it

is dissolved during the development step. In the meanwhile, non-irradiated part of the film remains insoluble. (5) This step is followed by a transfer and stripping steps (6).

2. Experimental section

2.1 Materials

Highly deacetylated chitosan (DA = 1%) was provided by Mahtani Chitosan PVT, Ltd (India) from squid pens and purified according to the Rinaudo procedure. [19] Chitosan was prepared by partial hydrolysis of chitin in alkaline medium. [20,21] A batch of this chitosan was reacetylated [22] to obtain a chitosan with higher degree of acetylation (DA). The obtained DA was 35% which was confirmed by ^{1}H NMR according to the Hirai procedure [23] using an AVANCE III 400 MHz spectrometer. After reacetylation, the average weight molar mass (M_w) and average molar mass (M_n) were measured by size exclusion chromatography. They were estimated to be 705 kg.mol^{-1} and 334 kg.mol^{-1} respectively (Dispersity Đ = 2.1). To prepare chitosan solutions deionized water and acetic acid (Merck, glacial acetic acid 99%) were used.

2.2 Thin films preparation and characterization

Aqueous diluted acetic acid solution 0.2 % (v/v) was used to dissolve chitosan flakes at a concentration of 0.7 % (w/w). The solution was left under magnetic stirring at room temperature until complete dissolution of chitosan. Silicon wafers were first rinsed with acetone and ethanol, then placed in an UV-ozone cleaner for 15 minutes to remove any organic pollutants and to increase the polarity of the substrate for better adhesion of the chitosan film. Films were deposited by spin-coating for 60 s at 3000 rpm with acceleration of 600 r/s^2 followed by a soft bake at 150°C during 5 min on the hotplate. Typical film thickness under these spin-coating conditions was ±100 nm. Measurements of the films thickness were performed by spectroscopic ellipsometry using a UVISEL ellipsometer from Horiba-Jobin-Yvon (spectral range 190 – 830 nm). Obtained data were fitted using New Amorphous model with the software from the UVISEL ellipsometer.

2.3 Size Exclusion Chromatography (SEC)

Self-supported thick films (5 microns) were prepared by casting and drying (60°C, 2 h) the same chitosan solution in a glass mold. The resulting chitosan films were then dissolved at 0.5 mg/mL in a 0.2 M acetic acid/0.15 M ammonium acetate buffer (pH 4.5) during a minimum of 18h at ambient temperature. The solutions were then filtered using 0.45 µm pore size CME membranes (Millipore).

The average molar masses (M_w and M_n) and the dispersity Đ of chitosan in each film were determined by size exclusion chromatography (SEC). The polymer separation was

performed on two serially connected columns (TSK G2500PW and TSK G6000PW, TOSOH BIOSCIENCE). A differential refractometer (Optilab T-rex, WYATT) coupled on-line with a MALLS detector (Dawn Heleos II, WYATT) was used for the detection. A degassed 0.2 M acetic acid/0.15 M ammonium acetate buffer (pH 4.5) was used as eluent after filtration on a 0.10 µm pore size membrane (Millipore). The flow rate was maintained at 0.5 mL/min and the amount of sample injected was 50 µL. The refractive index increment (dn/dc) was adjusted for each acetylation degree (DA) according to the results of Schatz et al. [24]

2.4 Photostructuration

For the DUV exposure, an Excistar (Coherent) nanosecond ArF Excimer laser emitting at 193 nm was used. The exposure time was controlled with a mechanical shutter. A beam expander was used to expand and homogenize the beam. The sample was located at a stage, motorized in x,y and z. Lithography was followed by development in aqueous solutions of various pH: 0.02 % (v/v) acetic acid (pH = 4), deionized water (pH = 7) and 10^{-4} M NaOH solution (pH = 10). Developing time was 30 s.

Additional tests on a commercial 193 nm stepper were carried out. For this, a 300mm coat & develop track SOKUDO DUO (SCREEN) was used. The exposure tool was an ArF dry scanner Nikon NSR307E at NA 0.85.

2.4 Plasma etching

Silicon wafers (thickness of 500 µm) with 200 nm thick CVD SiO_2 layer were used. Patterns written in the chitosan layer were transferred into the underlying silica using a reactive ion etcher (RIE Corial 200S) operating under the conditions described in Table 1. The etching process was composed of three etching steps: first an oxygen Descum plasma to remove the remaining chitosan at the bottom of the features after development, then the silica etching with CHF_3 plasma and finally a stripping step to remove the chitosan mask layer.

Table 1: Successive etching conditions using the RIE Corial 200S for transferring patterns in the chitosan layer into the underlying silica.

Step	Gaz	Flow gaz (sccm)	Pressure (mT)	RF Power (W)	Time (s)
Descum	O_2	40	100	40	5
Etching	CHF_3	100	50	140	45
Stripping	O_2	100	100	100	120

2.5 Temperature Programmed Desorption coupled to Mass-Spectrometry (TPD-MS)

In order to characterize the thermal processes induced in the chitosan thin film, home-made temperature programmed desorption set-up connected to a mass-spectrometer was used. Two silicon wafers with spin-coated chitosan film were placed in a fused silica tube in a vacuum system. Samples were heated from 25°C to 600°C with a heating rate of 5°C/min. The gases emitted during the heating process were continuously analyzed by a mass-spectrometer.

2.6 Contact angle measurements

Contact angle measurements were performed using a KRÜSS DSA 100 goniometer (Germany). Deionized water droplets were put on the film surface and the acquisition data were recorded immediately using the ADVANCE software. The contact angle was calculated automatically. The measurement process was repeated four times.

2.7 Fourier transform infrared (FTIR) spectroscopy

The FTIR spectrum of chitosan film was recorded on a Thermo Scientific Nicolet 8700 spectrometer. Film was deposited on the thin silicon wafer (thickness around 250 μm). Transmission mode was used to collect the data. Spectra were taken with a resolution of 4 cm^{-1} and were averaged over 32 scans in the range 4000 – 500 cm^{-1}.

2.8 XPS

The XPS analysis was performed on a Gammadata Scienta (Uppsala, Sweden) SES 200-2 X-ray photoelectron spectrometer under ultrahigh vacuum conditions ($P < 10^{-7}$ Pa). CASAXPS (Casa Software Ltd, Teignmouth, UK, www.casaxps.com) was used to fit all the peaks and area of each component of XPS data.

2.9 ToF-SIMS

ToF-SIMS measurements were carried out on a TRIFT III ToF-SIMS instrument (Physical Electronics, USA) operated with a pulsed 22 keV Au^+ ion gun (2 nA ion current) rastered over a 300 × 300 μm^2 area. The electron gun was operated in pulsed mode at low electron energy for charge compensation. The ion dose was kept below the static conditions limit. Data were analyzed using the WinCadence software. Mass calibration was performed on hydrocarbon secondary ions. Mean values and standard deviations for some intensity ratios and normalized intensities were calculated from data obtained on three analysis areas.

Normalization in the positive mode was performed on the total positive ion intensity from which were subtracted the intensity values of H^+ (due to possible changes as a function of very slight changes in the experimental settings), Na^+, K^+, Ca^+, PDMS main peaks (at m/z = 27.98, 73.05, 147.07, 207.03, 221.09, 281.05, 325.02 and 355.07). Similarly, normalization in the negative mode was performed on the total negative ion intensity from which were subtracted the intensity values of H^- (due to possible changes as a function of very slight changes in the experimental settings), F^-, $^{35}Cl^-$, $^{37}Cl^-$, alkyl sulfate related peaks (SO_x^-, $C_{14}H_{29}O_3S^-$, $C_{15}H_{31}O_3S^-$ and $C_{16}H_{33}O_3S^-$), PDMS main peaks (at m/z = 27.98, 73.01, 75.00, 89.04, 91.02, 149.01, 163.06, 165.04, 223.03 and 237.08).

2.10 Atomic Force Microscopy (AFM)

The microstructured films were characterized using atomic force microscopy (AFM) in the tapping mode, using a PicoPlus 5500 System model from Agilent. Scanning was performed at 1 line/sec with an image resolution of 512 x 512 pixels.

3. Results and discussion

3.1. Effect of DUV on chitosan chains

The use of chitosan as a positive photoresist assumes that irradiation can generate a significant change in film solubility. In the case of chemical amplification resins, which are widely used in microelectronics today, this change is achieved by a modification of the polarity of the polymer chains constituting the resin, which makes the resin soluble in the developing solvent. Thus, resins are specifically designed by incorporation of appropriate monomers within the macromolecules to confer this solubility. The strategy of our work is based on the use of chitosan without chemical modification. The behavior of chitosan under DUV irradiation is thus observed in a first step.

Spectroscopic ellipsometry was used to characterize the thickness and optical properties of the chitosan thin film after spin-coating. The results are shown in **Figure S1** in Supporting Information. Spin-coating parameters were chosen to obtain a film thickness of 100 nm ± 2 nm. This thickness can easily be adapted by modifying the spin-on deposition conditions, while maintaining the quality of the deposited films (see **Figure S2** in Supporting Information). The optical data show a high transparency of the polysaccharide for wavelengths above 300 nm. At 193 nm, k equals to 0.0624. This value corresponds to 30-35 % of the light absorbed at 193 nm for a 100 nm thick film. This corresponds to an absorption coefficient α=3.57 μm^{-1}. Compared to standard commercial 193 nm photoresist (typ. 1 to 3 μm^{-1}) [25,26,27] this value is thus slightly superior but such absorption coefficient guarantees a light penetration through the whole film, and at the same time, part of the light is absorbed and can eventually modify the properties of the resin, opening possibilities towards photolithography applications.

The absorbance of chitosan at 193 nm allows to envision that modifications of the molecular structure of chitosan can be expected after DUV irradiation, opening the door to applications in DUV photolithography, as it has been shown on other organic [28,29,30] or organic-inorganic hybrid materials. [31,32,33]

The modification of chitosan under DUV irradiation was first investigated by size exclusion chromatography to reveal a possible change in macromolecular chain size (**Figure 2**). To have a sufficient amount of polymer to analyze, self-supported thick films (5 microns) were prepared using the same chitosan solution (**Figure 2.d**). Three DUV doses were used: 1000, 5000 and 10000 mJ/cm^2. The 1000 mJ/cm^2 dose is a required value for photolithography. Higher doses were envisaged to take into account the fact that the thickness of the film is much

more important than for the applications in photolithography. For thick films, the internal filter effect cannot be neglected.

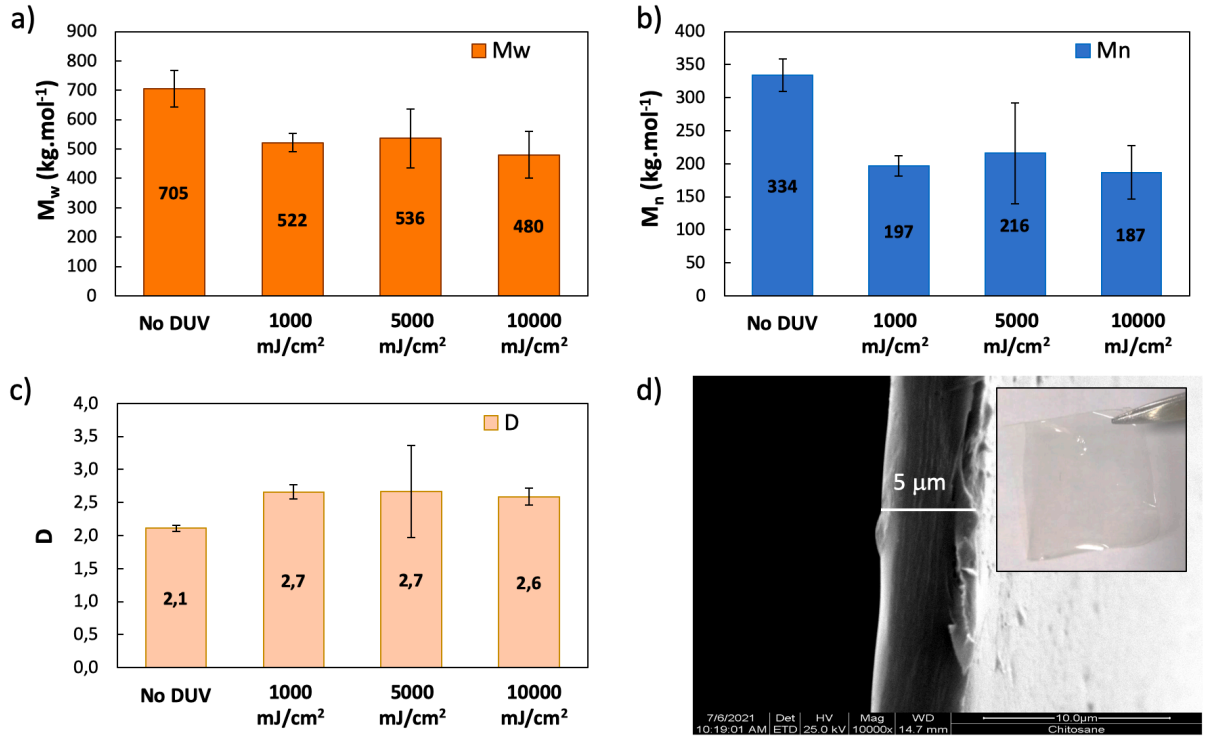

Figure 2. SEC characterizations of chitosan films (5 microns), before and after DUV irradiation with different doses. The results of a) M_w, b) M_n and c) Đ are presented as well as d) a photograph of the self-supported film and a SEM image of the section.

A significant decrease of M_w and M_n (displayed in **Figure 2.a** and **Figure 2.b**, respectively) is observed after 1000 mJ/cm^2, which proves that DUV irradiation causes chitosan chains to split. Longer irradiation does not accentuate the phenomenon but one can imagine that the strong absorption of chitosan at 193 nm prevents the modification of the deeper layers. As expected, the dispersity Đ (**Figure 2.c**) increases with irradiation at 1000 mJ/cm^2 and then remains stable, confirming the production of smaller chains but with only partial conversion in the film thickness.

In order to go further in understanding the impact of DUV on chitosan thin films, FTIR analysis was used to follow the modification of main functional groups present in the chitosan structure. The FTIR transmission spectrum (**Figure 3**) of the chitosan film may be divided into three main regions:

1. A region between 3500 cm^{-1} and 2500 cm^{-1} which is a broad asymmetric band that includes C – H stretching bands registered at 2880 cm^{-1} and 2940 cm^{-1} and axial O – H and N – H stretching centered at 3440 cm^{-1}.
2. A region between 1700 cm^{-1} and 1200 cm^{-1} encompassing the C = O stretching (amide I) at 1645 cm^{-1}, N – H bending (amide II) at 1558 cm^{-1} and C – N stretching (amide III) at 1323 cm^{-1}. [34] The sharp peaks at 1381 cm^{-1} and 1412 cm^{-1} can be assigned to the CH_3 symmetrical deformation mode. [35]
3. A "fingerprints" region, the area of overlapping peaks between 1200 cm^{-1} and 940 cm^{-1}. The strong absorption is due to skeletal signals (vibrations of glycosidic bonds, variety of C – O – C and C – O single bond vibrations), which is a characteristic of chitosan polysaccharide structure. [36]

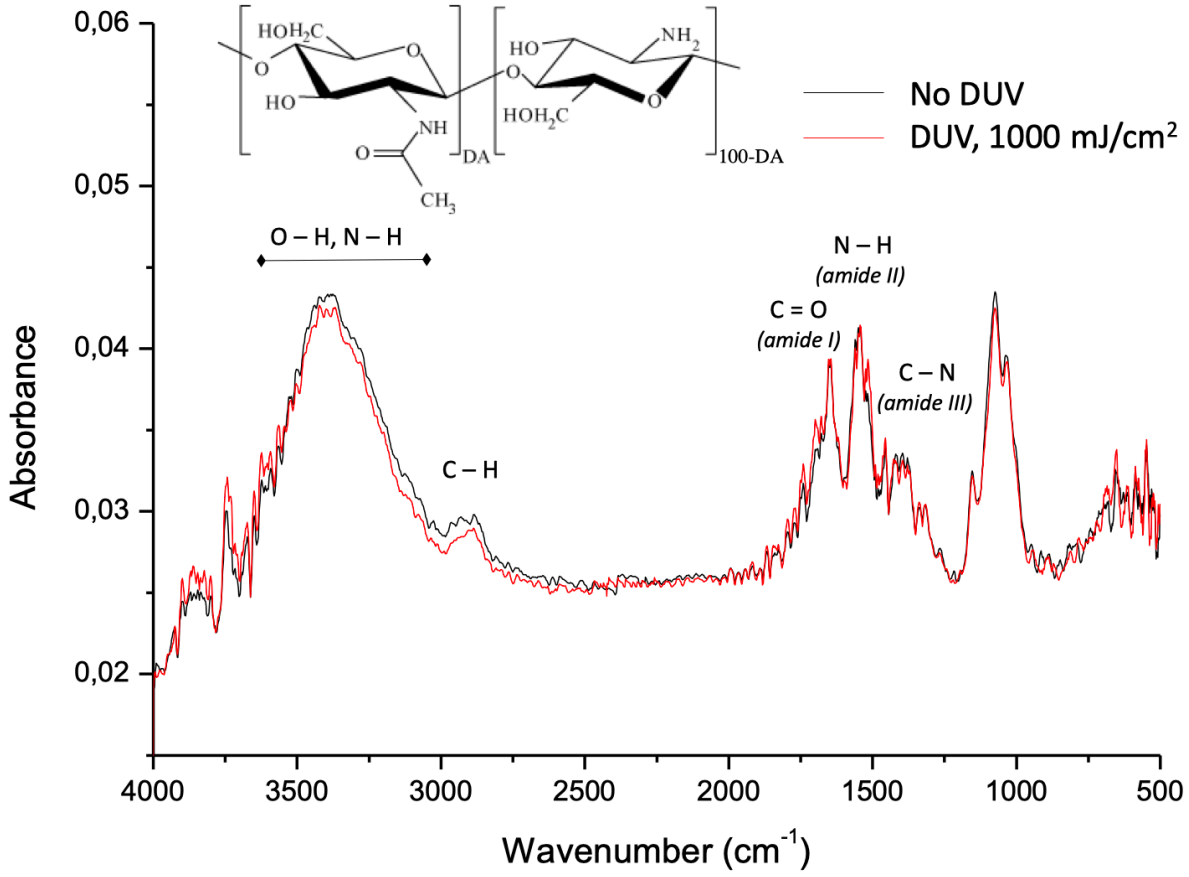

Figure 3. FTIR transmission spectra of chitosan film on the Si wafer collected in transmission mode. Irradiation dose was 1000 mJ/cm^2.

The comparison of FTIR spectra before and after irradiation shows a remarkable stability of the chitosan films. Indeed, no significant modifications of the characteristic bands

of chitosan were observed after an irradiation with the dose of 1000 mJ/cm^2. It is concluded that the amide groups are stable under DUV irradiation. These results are in line with previous results obtained by Sionkowska et al, [37] where chitosan was irradiated at 248 nm using a KrF laser. At the same time, Wasikiewicz et al. [38] affirm that after irradiation, the hydroxyl peak increases, while the C – O – C peak decreases. Therefore, in our case, it may be hypothesized that under irradiation chain scissions occur at the glycosidic bonds followed by formation of hydroxyl group. This scission process may have a low extent which explains the low impact on the FTIR spectrum. However, the modification of molar mass leads to a significant increase in solubility for the chitosan that can be used for patterning as shown below.

To support this hypothesis on the molecular mechanism, XPS, water contact angle and ToF-SIMS analysis were conducted. The XPS spectrum of the non-irradiated chitosan film is given in **Figure 4.a**. As expected, the peaks of C, O and N are found. The calculated ratio between those elements was 58.76%, 33.91% and 7.33% respectively. The C 1s peak of the non-treated chitosan film is resolved into five bonds. The peak at 285.00 eV was assigned to C – C or C – H bonds. The most intensive peak at 286.52 eV was assigned to C – OR chemical binding, the peak at 286.10 was due to C – N bond. At 288.09 two peaks were registered. The first one was assigned to C = O or O – C – O bond, while the peak with a lower intensity was assigned to O = C – N bonding. The O 1s spectrum was deconvoluted into three sub-peaks. The first one, at 533.14 eV was assigned to O – C – O chemical binding. The second one, at 532.82 eV was assigned to C – O or O – H or bound water. [39] And the last one, the least intensive peak at 531.64 eV was due to N – C = O binding. The N 1s spectrum required two peaks for the curve fit. The first peak at 399.58 eV was assigned to C – N – H or N – C = O bonds and the second one, at 401.62 eV to C – N^+ bond. The relative ratios are given in **Table S1**.

After the irradiation of the film with 1000 mJ/cm^2 (**Figure 4.b**) it is remarkable to notice that the ratio between C, O and N stays unchanged: 58.18%, 34.65% and 7.18% respectively. Neither the position, nor the peak area of the C 1s, O 1s or N 1s spectra changed. Thus, it is concluded that the molecular chemistry of chitosan at the surface of the film is not affected by DUV irradiation. The solubility change of the film must come from the chain scission which cannot be detected by means of XPS.

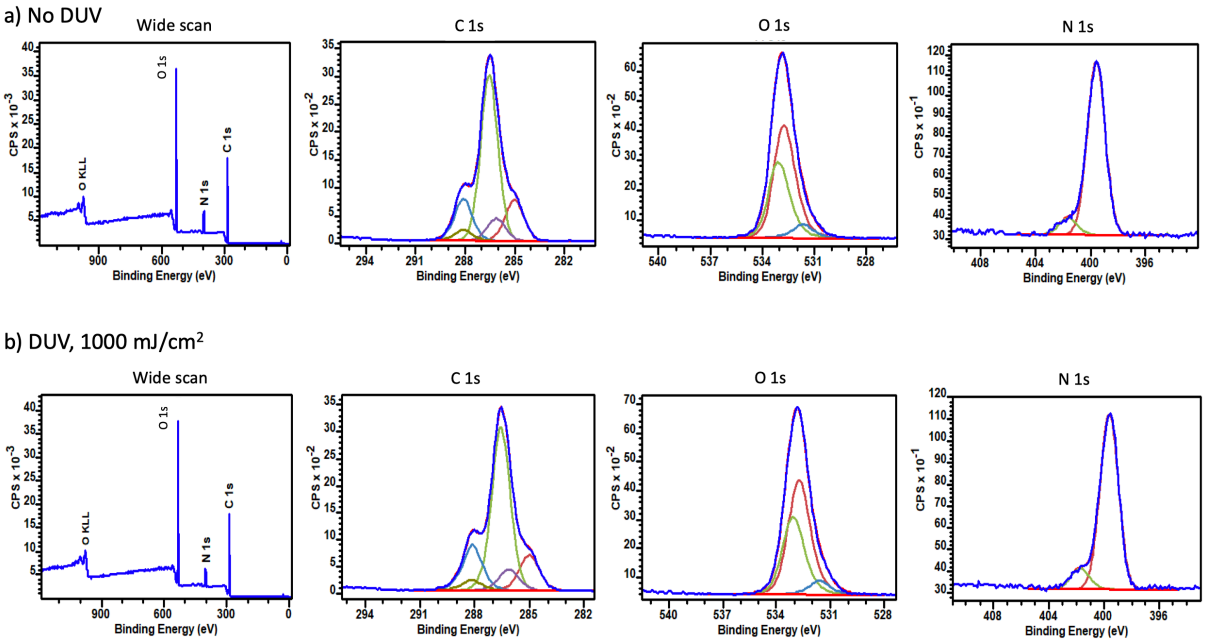

Figure 4. XPS spectra of the chitosan film a) before and b) after 1000 mJ/cm^2 DUV irradiation. Wide scan spectra, and deconvolution C 1s, O 1s and N 1s peak are plotted.

These surface characterization results were confirmed by surface energy measurements. Contact angle measurements were performed to characterize the non-covalent forces between the liquid (DI water) and the chitosan film. Since the film can be dissolved by a water drop, the measurements were taken after the first seconds of liquid/film contact (**Figure S3** in Supporting Information). There is no significant change of the contact angle with water (33.2 ± 1.4 to 35.3 ± 1.3 after irradiation with 1000 mJ/cm^2), confirming the chemical stability of chitosan under DUV.

The effect of 193 nm irradiation is thus different from 248 nm irradiation, reported by Sionkowska et al [37]**.** They showed that after the irradiation at 248 nm using KrF excimer laser, the surface polarity increases which may be caused by photooxidation. This increase was explained by the photodestruction of glycosidic bonds. This chemical modification was obtained after a long irradiation time (at least 2 hours), which may reveal that such a process has a slow kinetics and why it was not observed in our irradiation conditions. This may also explain why in the DUV irradiation conditions used here, we did not observe the photooxidation of the polymer film detected for other polymers. [40]

Complementary characterization was performed using ToF-SIMS as it was expected that the mass related molecular information could bring more detailed insight on the mechanism. ToF-SIMS spectra in positive mode are very similar (see **Figure 5**), which is consistent with the results from the other characterization techniques. These spectra exhibit

secondary ions related to the chemical structure of chitosan at low mass (see CH_2-NH_2^+ detected at m/z = 30.04 and CH_2-OH^+ detected at 31.02) and more specific molecular signatures at m/z >100 such as peaks at m/z = 112.04, 126.06, 138.06, 144.07, 162.08 (see peak identification in the Figure). This is similar to results from the literature. [41] Signatures related to low levels of contamination (PDMS, alkyl sulfates) are also detected (see details in the experimental section). Results in the negative mode are also very similar (not shown).

As the spectra look very similar, a more detailed study was performed by comparing various intensity ratios and normalized intensities of interest. Normalization considered all possible slight variation sources due to settings and contamination to make possible the most precise comparison. **Table 2** exhibits some of the comparison parameters. Values are very similar, confirming that the functional groups are intact (as already indicated by other characterization techniques). Some parameters do not exhibit any significant difference (such as normalized intensities for CH_2-OH^+ and for CN^-) but others do (such as the O^-/CH^- ratio and normalized intensities for CH_2-NH_2^+ and for high mass specific molecular signatures in the positive mode). This might indicate a structural change, such as some chain scissions, that might have influenced the creation of secondary ions in the ToF-SIMS analysis and then consequently their relative intensities in the spectra.

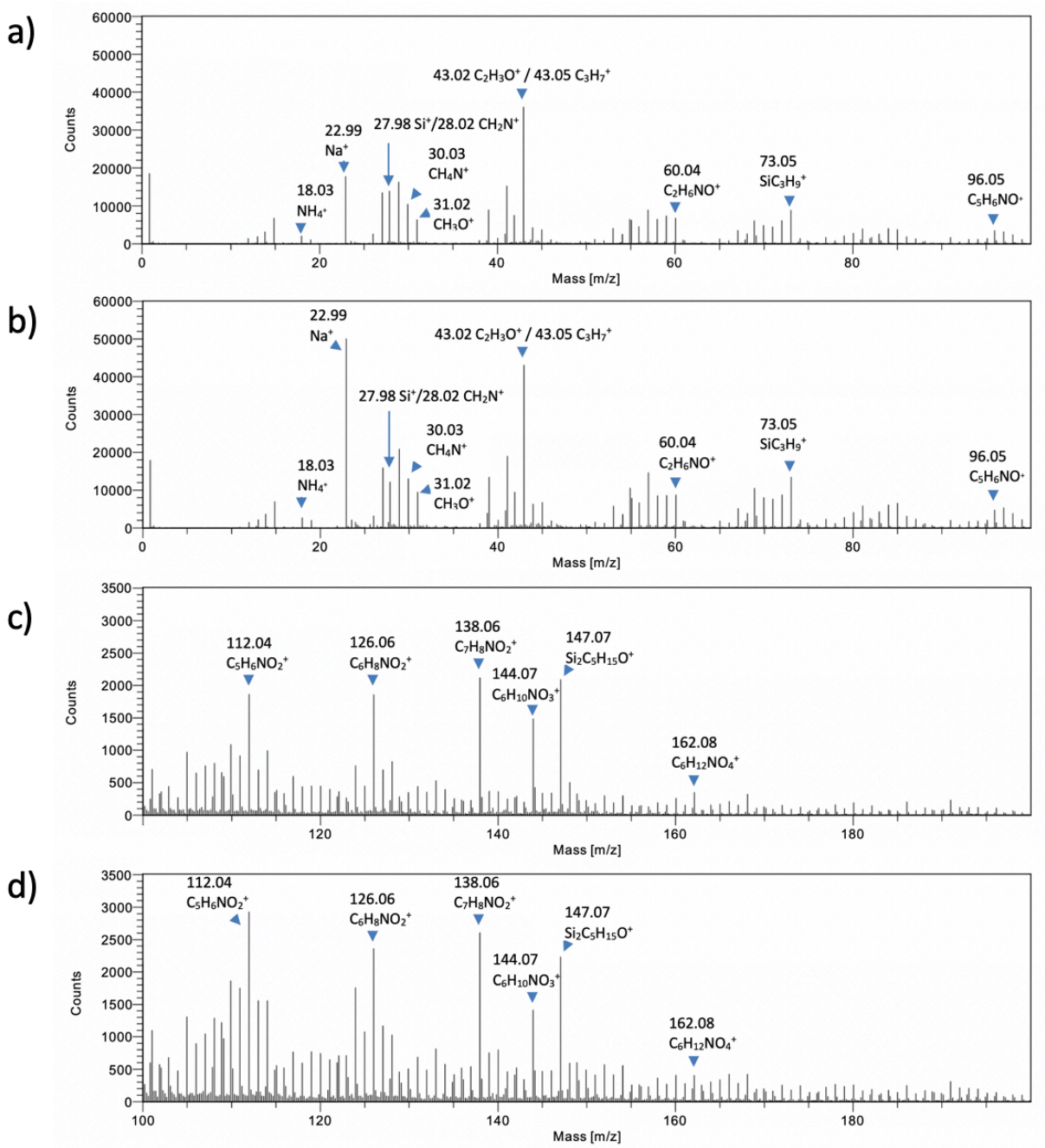

Figure 5. ToF-SIMS positive ion spectra of the chitosan film (a) and (c) before and (b) and (d) after 1000 mJ/cm^2 irradiation. (a) and (b) : 0-100 m/z range; (c) and (d) : 100-200 m/z range.

Table 2. ToF-SIMS intensity ratios and normalized intensities (‰) of interest on chitosan films before and after irradiation (1000 mJ/cm^2)

Sample	CH_2-NH_2^+	CH_2-OH^+	High mass positive ions *	O^-/CH^-	CN^-
Non-irradiated film	22.1 ± 0.7	13.8 ± 1.6	21.6 ± 2.2	2.3 ± 0.1	43.6 ± 3.1
Irradiated film	19.3 ± 0.2	14.2 ± 1.1	18.5 ± 0.2	2.9 ± 0.1	47.3 ± 2.3

* at m/z = 112.04, 126.06, 138.06, 144.07, 162.08

In conclusion of this part, the different analysis techniques used show that chitosan undergoes, under DUV irradiation, a decrease of its molecular size, but without chemical structure denaturation. In the following, we demonstrate that it is possible to use this depolymerisation to show the use of this biosourced material for photolithography applications, with a behavior of the resin as a positive resin, and by integrating at the same time the photostructuring step and the transfer by etching.

3.2 DUV photopatterning

In a first step, the post-exposure process and development conditions must be defined. To qualitatively observe the behavior of chitosan under DUV irradiation, 124 ± 2 nm thick chitosan films were irradiated through a binary chromium mask with a 10 µm period. Three irradiation doses were chosen: 300 mJ/cm^2, 600 mJ/cm^2 and 900 mJ/cm^2. This range of dose covers the doses used for photopatterning, as shown in more details below. After irradiation, the film was immersed in a developing solution to observe its solubility and in particular, to highlight differences between the irradiated and non-irradiated areas. Aqueous solutions of different pH were used: 0.2 % (v/v) acetic acid (pH = 4), deionized water (pH ≈ 7) and 10^{-4} M NaOH solution (pH = 10). Two different temperatures of post-applied bake (PAB) (100°C and 150°C during 5 min) were also tested. The process steps are schematized in **Figure 6.a**.

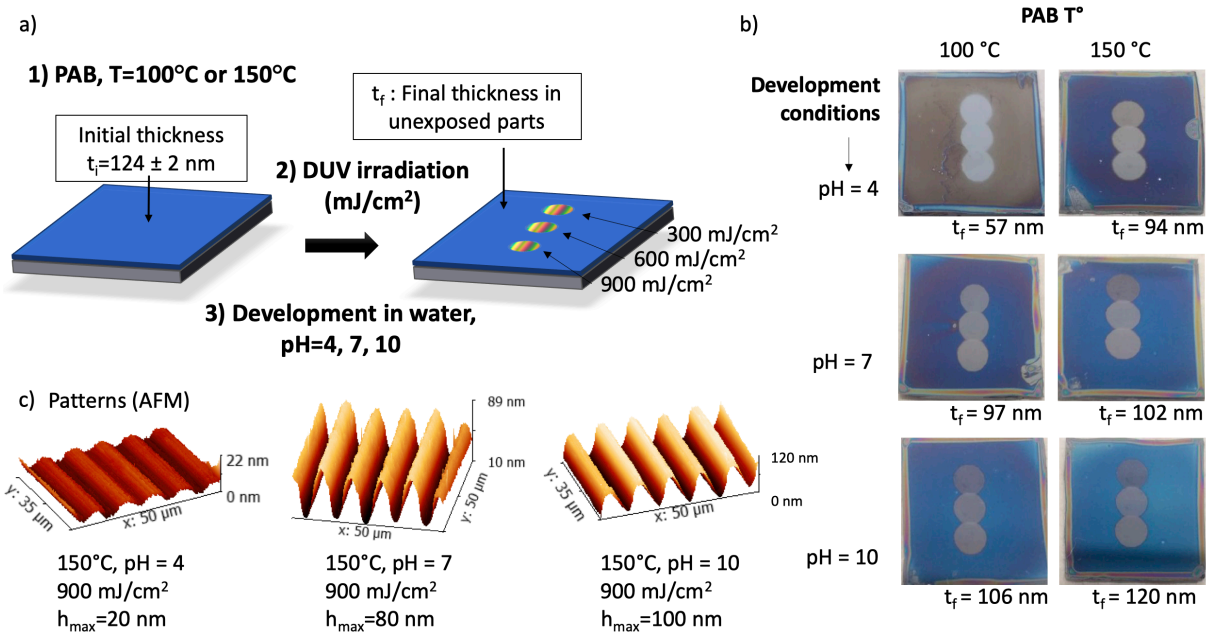

Figure 6. a) Schematic view of the photolithography process main steps. Initial thickness of the samples after PAB was chosen as 124 nm. b) Photographs of the samples after irradiation through binary mask with 300, 600 and 900 mJ/cm^2 exposure conditions, PAB at 100°C or 150°C (5 min) and development in aqueous solution with pH = 4, 7 or 10. c) Typical AFM images recorded for different process conditions.

The film thickness of the non-irradiated zones was measured before and after development. AFM scans were made for the irradiated zones after development. These are resumed with photographs of the samples after treatment in **Figure 6.b**. The final thickness of the film in the non-irradiated parts (t_f) is also given. This value has to be compared to t_i, the initial thickness of the film after PAB. An optimized positive tone resist should keep this value constant in the process.

Regardless of the conditions for the film treatment after exposure, it was found that the irradiated areas appear clearly, highlighting a change in film thickness in the irradiated areas. This behavior corresponds to the positive photoresist properties that is sought. As shown in previous section, DUV irradiation provokes a decrease of the M_w. It was already reported that smaller molecular weight chitosan dissolves faster than higher molecular weight chitosan, [42,43] which can account for the positive tone photoresist properties of chitosan under DUV irradiation.

For the acid developing solution (pH =4) and a soft-bake temperature of 100°C, we observe a partial redissolution of the film in the non-exposed parts. The thickness is indeed divided by two under these conditions (124 nm to 57 nm). AFM in the patterned part reveals

that the microstructures are not visible with such conditions. These conditions are not appropriate for the intended application. When the soft-bake temperature increased to 150°C, the resistance of the film to acidic conditions is stronger but the loss of thickness in the non-irradiated areas is about 25% (124 nm to 94 nm). In the irradiated areas, the pattern features are visible (**Figure 6.c**, left image) but their height (about 20 nm) is significantly lower than the initial thickness of the film, for the 3 selected doses. The development conditions in acidic pH are therefore not adapted, despite the film densification step by soft-bake. This result is in fact expected due to the solubility of chitosan in acidic medium.

In the neutral developing solution (pH = 7), the non-irradiated area of the sample is more resistant to development, even though film shrinkage was observed for both soft-bake temperatures. Final thickness t_f is 97 and 102 nm for 100°C and 150°C PAB respectively. As for the acid developing solution, the film annealed at 150°C was less soluble than at 100°C. However, for both temperatures, the patterns were well revealed and maintained in the irradiated zones. A typical example is given in **Figure 6.c** (center image). The microstructure height was found as 80 nm, which is less than the total film thickness. This means that the upper part of the non-irradiated chitosan film is dissolved during the development. However, this value was proved to be sufficient for transfer by etching as shown below.

The dissolution of the film was less marked in the alkaline medium, in particular the film thickness after development of the 150 C° soft-bake sample (120 nm) was close to the original one (124 nm). At the irradiated zones, patterns were well defined, which makes these conditions interesting for photopatterning **(Figure 6.c**, right image). However, NaOH solution as a developer cannot be used in the lithographic processes as Na^+ ions are considered as pollutant in microelectronics.[44]

Consequently, deionized water was chosen as an optimal developer since it perfectly fits into the framework of green lithography and allows achieving satisfying results. Also, 150°C was set as a soft-bake temperature as it increases the resistance of the film during the development step. Next, thermal degradation studies of chitosan thin films were conducted to address whether these soft bake conditions induce molecular modification of the polysaccharide.

TPD-MS and TGA were used to verify that the chosen temperature (150°C) was low enough to avoid any thermal degradation of the chitosan thin film. The TPD-MS thermograms (**Figure S4** in Supporting Information**)** show that from 50°C to 300°C the main process is the desorption of water. Desorption of CO_2 and CO contaminants occurs from 75°C to 300°C and from 175°C to 300°C respectively. From 300°C to 400°C several signatures can be seen: H_2,

N_2, NO and CH_4. Obtained results are in a good agreement with those observed by Leceta *et al.*[26] who reported that degradation of the chitosan starts from 290°C. For temperature below this limit, the weight loss was caused by the loss of moisture. TGA analysis of the chitosan film (**Figure S5** in Supporting Information) also shows that there is a slight weight loss (11,6%) at temperatures below 280°C which can be attributed to loss of moisture and bound water.[34] The main loss of weight starts after 280°C where the degradation of the chitosan takes place. Therefore, the obtained results confirm that the chosen PAB temperature of 150°C does not thermally degrade the chitosan film. This condition was thus used in the following.

The photopatterning of the chitosan at 193 nm was thus studied in more details with the irradiation doses ranging from 10 mJ/cm^2 to 900 mJ/cm^2. Binary chrome mask with 10 µm line pattern was used to separate the exposed and unexposed zones. After irradiation, the samples were developed in deionized water for 30 s. The results are plotted in **Figure 7**.

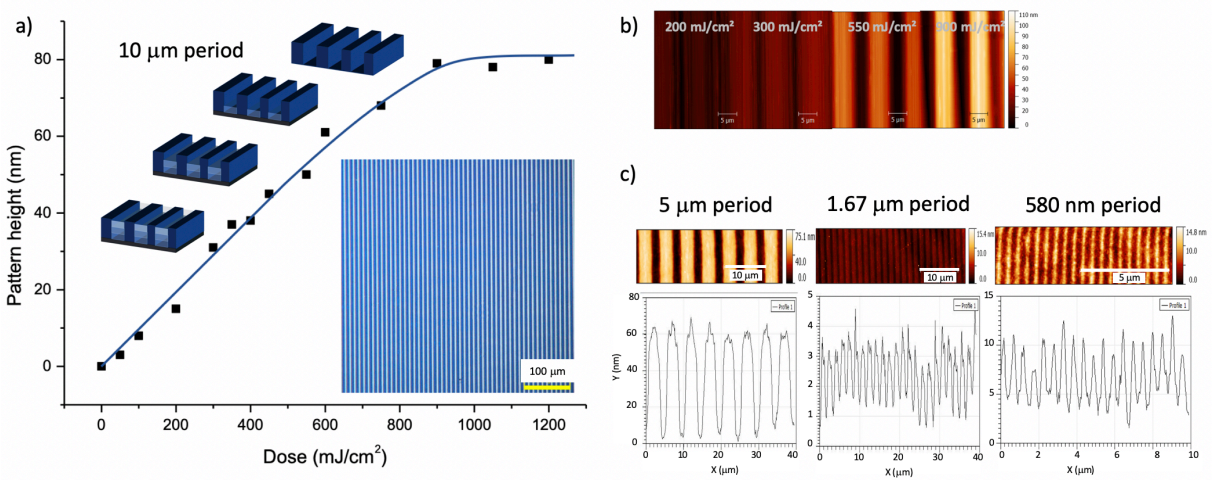

Figure 7. a) Evolution of pattern height (10 µm period) with DUV dose. Initial thickness was 100±2 nm, PAB: 150°C, development in deionized water (pH = 7) for 30 sec. The inset is a wide area view by optical microscopy showing the homogeneity of the sample. b) AFM images for 200, 300, 550 and 900 mJ/cm^2. c) Example of patterns obtained with other masks with period of 5, 1.67 and 0.58 µm.

Patterns appear at dose under 100 mJ/cm^2. With the increase of the dose, the pattern depth increases linearly, which corresponds to the progressive photomodification of the chitosan in the irradiated parts. The optimal dose was 900 mJ/cm^2, which allows obtaining 80 nm height patterns after development (**Figure 7.b**). From analysis of AFM images, it was concluded that no remaining chitosan was detected between lines. The difference with the nominal height of

the chitosan film was explained by a loss of materials in the non-exposed parts during development. For doses higher than 900 mJ/cm^2, no more difference was observed, which justifies the definition of the optimal dose at 900 mJ/cm^2.

Patterns with smaller lateral dimensions were also obtained, as shown in **Figure 7.c**. In the case of 5 µm width patterns, the maximum height was slightly lower (70 nm), due to residual chitosan layer between lines. Submicrometric resolution was also proven (580 nm width). However, in this case, the pattern height was significantly lower than the initial film thickness (100 nm). This may be due to the interferometric lithography setup that is used and the linear response of the chitosan photoresist. Indeed, in this case, a sinusoidal light pattern is used and thus it is challenging to obtain the maximum photoresist contrast.

3.3 Towards photolithography industrial applications

Finally, in order to demonstrate the interest of chitosan as a green resist for microelectronic applications, we show that the compatibility of this resist with 300 mm industrial line included spin-coating and 193nm scanner photolithography tools.

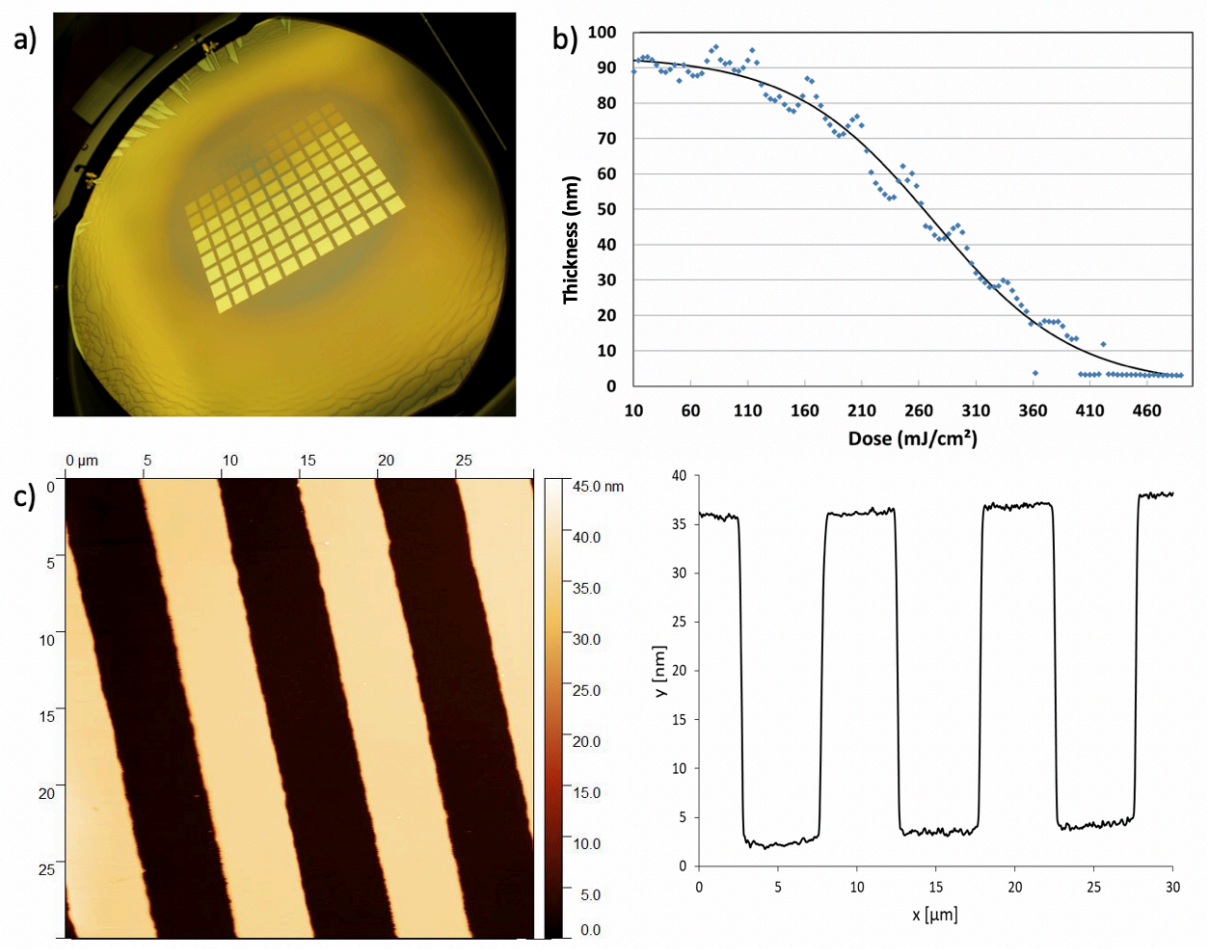

Figure 8. a) Photograph of a chitosan film deposited on a 300 mm Si wafer and exposed with 193nm dry scanner. b) Associated contrast curve plotted after thickness measurement on this sample. c) AFM Image and profile of 5 µm wide lines (spaced of 5 µm) of chitosan patterns transferred into silica hardmask layer after plasma etching.

Figure 8.a shows a photograph of a 100 nm chitosan layer deposited by spin-coating on a 300 mm Si wafer and exposed with incremental doses from 10 to 490 mJ/cm² (step 4 mJ/cm²). The spin-coating parameters of the chitosan film have to be optimized on the wafer edges to fully cover the wafer. However, the quality of the central part of the wafer (200 mm) was sufficient to assess the exposure with a commercial ArF dry scanner. The contrast curve presented in **Figure 8.b** confirms the photosensitivity of the chitosan film at 193 nm irradiation. The dose-to-clear is of the order of 400 mJ/cm² with a contrast of $\gamma \approx 1.6$. This value is therefore of the same order of magnitude as the optimal dose value shown in **Figure 7**. The difference comes from the different type of irradiation and the incident power density measurement. These results also validate the development performed in deionized water of pH = 7.

The possibility of transfer by physical etching is also shown. This step is crucial to consider industrial applications in the microelectronic field. In particular, it is important to prove that the chitosan used for its properties in photopatterning is suitable for this step. Empirical Ohnishi number was determined for the chitosan that we used, by using the Ohnishi equation. [44] A value of 10.3 was obtained. 5µm wide lines spaced by 5µm were patterned in the chitosan layer using the 193 nm radiation. As shown previously, for 5 µm patterns, a thin residual chitosan layer remained in the exposed area. Therefore, a soft oxygen plasma (Descum) has been done to etch this residual layer while keeping enough resist for the transfer. Indeed, after the Descum step, approximately 50% of the chitosan protective layer (unexposed area) remained and its thickness was then 40 nm. Silica etching was done by CHF_3 and the etch time was set to 45 sec. After the silica etching step the remaining chitosan thickness was 25nm. Finally, the remaining chitosan was removed during the stripping plasma. **Figure 8.c** shows an AFM image and a profile of the resulting patterns transferred into the silica layer after stripping. Under our conditions, the etching rate of chitosan was 20 nm/min and the one of silica was around 40 nm/min (selectivity of 2) leading to 30 nm deep features. Their width was 4.96 ± 0.05 µm and deviated by less than 1% from the expected value. The fidelity of the motifs has been respected. Finally, Root Mean Square (RMS) surface roughness at the top and bottom of the features were 0.4 nm.

4. Conclusions

In this paper, we demonstrate that chitosan can be considered as a starting biosourced material to formulate positive photoresists for microelectronics. The photoinduced mechanisms between the 193 nm laser beam and the polysaccharide have been extensively studied and show remarkable stability of the surface and core properties of chitosan. Nevertheless, a photoinduced decrease of the chitosan molar mass induces a difference in solubility between the insolated and non-insolated areas. This study focused on the photolithography step with intermediate resolutions and especially the compatibility with industrial tools and the possibility to use chitosan patterns as physical transfer masks. This work opens important perspectives to reduce the ecological impact of processes used in microelectronics. Work is in progress to increase the sensitivity of the resin and to optimize the etching parameters to make this green resist as performant as the standard photoresists. In particular, the sensitivity of the chitosan photoresist should be improved significantly to be compatible with microelectronic industry standard. Use of a photoacid generator will be assessed so as to reach this objective. In addition, a new door is opened to structure chitosan films at different scales, which also opens up perspectives in optics, photonics and structured biosurfaces for medicine and biology.

Supporting Information

Optical characterization of chitosan thin films, Spin-coating calibration curves, Atomic composition from XPS characterization, Contact angles of water on chitosan films after DUV treatment, TPD-MS data, TGA data.

Acknowledgments

The authors thank the Agence Nationale pour le Recherche (ANR) for funding this project (Project Lithogreen, Grant ANR-19-CE43-0009). Benjamin Leuschel, Samar Hajjar, Philippe Kunemann, Gautier Schrodj and Agnès Crépet are gratefully acknowledged for their technical assistance in the DUV lithography, XPS, surface energy, thermal measurements experiments and SEC respectively.

References

(1) Chung, J.; Choi, J.; Chung, S. Pilot study of specific microbe immobilization cells (SMICs) technology in removing tetramethyl ammonium hydroxide for reuse of low-strength electronics wastewater. *J. Hazard. Mater.*, **2020**, *384*, 120829.

(2) Hu, T.-H.; Whang, L.-M.; Liu, P.-W.G.; Hung, Y.-C.; Chen, H.-W.; Lin, L.-B.; Chen, C.-F.; Chen, S.-K.; Hsu, S.F.; Shen., W. Biological treatment of TMAH (tetra-methyl ammonium hydroxide) in a full-scale TFT-LCD wastewater treatment plant. *Bioresour. Technol.*, **2012**, *113*, 303-310.

(3) Lin, C.-C.; Yang, C.-C.; Ger, J.; Deng, J.-F.; Hung, D.-Z. Tetramethylammonium hydroxide poisoning. *J. Clin. Toxicol.*, **2010**, *48(3)*, 213-217.

(4) Takei, S.; Hanabata, M.; Oshima, A.; Kashiwakura, M.; Kozawa, T.; Tagawa, S. EB and EUV Lithography Using Inedible Cellulose-Based Biomass Resist Material; Hohle, C. K., Younkin, T. R., Eds.; San Jose, California, United States, 2016; p 977929. https://doi.org/10.1117/12.2217481.

(5) Takei, S.; Oshima, A.; Sekiguchi, A.; Yanamori, N.; Kashiwakura, M.; Kozawa, T.; Tagawa, S. Electron Beam Lithography Using Highly Sensitive Negative Type of Plant-Based Resist Material Derived from Biomass on Hardmask Layer. *Appl. Phys. Express* **2011**, *4* (10), 106502. https://doi.org/10.1143/APEX.4.106502.

(6) Takei, S.; Sugino, N.; Hanabata, M.; Oshima, A.; Kashiwakura, M.; Kozawa, T.; Tagawa, S. Ecofriendly Ethanol-Developable Processes for Electron Beam Lithography Using Positive-Tone Dextrin Resist Material. *Appl. Phys. Express* **2017**, *10* (7), 076502. https://doi.org/10.7567/APEX.10.076502.

(7) Jiang, B.; Yang, J.; Li, C.; Zhang, L.; Zhang, X.; Yang, P. Water-Based Photo- and Electron-Beam Lithography Using Egg White as a Resist. *Adv. Mater. Interfaces* **2017**, *4* (7), 1601223. https://doi.org/10.1002/admi.201601223.

(8) Dore, C.; Osmond, J.; Mihi, A. A Water-Processable Cellulose-Based Resist for Advanced Nanofabrication. *Nanoscale* **2018**, *10* (37), 17884–17892. https://doi.org/10.1039/C8NR04851G.

(9) Jiang, J.; Zhang, S.; Qian, Z.; Qin, N.; Song, W.; Sun, L.; Zhou, Z.; Shi, Z.; Chen, L.; Li, X.; Mao, Y.; Kaplan, D. L.; Gilbert Corder, S. N.; Chen, X.; Liu, M.; Omenetto, F. G.; Xia, X.; Tao, T. H. Protein Bricks: 2D and 3D Bio-Nanostructures with Shape and Function on Demand. *Adv. Mater.* **2018**, *30* (20), 1705919. https://doi.org/10.1002/adma.201705919.

(10) Qin, N.; Qian, Z.-G.; Zhou, C.; Xia, X.-X.; Tao, T. H. 3D Electron-Beam Writing at Sub-15 Nm Resolution Using Spider Silk as a Resist. *Nat. Commun.* **2021**, *12* (1), 5133. https://doi.org/10.1038/s41467-021-25470-1.

(11) Pennacchio, F. A.; Casale, C.; Urciuolo, F.; Imparato, G.; Vecchione, R.; Netti, P. A. Controlling the Orientation of a Cell-Synthesized Extracellular Matrix by Using Engineered Gelatin-Based Building Blocks. *Biomater. Sci.* **2018**, *6* (8), 2084–2091. https://doi.org/10.1039/C7BM01093A.

(12) Koev, S. T.; Dykstra, P. H.; Luo, X.; Rubloff, G. W.; Bentley, W. E.; Payne, G. F.; Ghodssi, R. Chitosan: An Integrative Biomaterial for Lab-on-a-Chip Devices. *Lab. Chip* **2010**, *10* (22), 3026. https://doi.org/10.1039/c0lc00047g.

(13) Lawson, R. A.; Robinson, A. P. G. Overview of Materials and Processes for Lithography. In *Frontiers of Nanoscience*; Elsevier, 2016; Vol. 11, pp 1–90. https://doi.org/10.1016/B978-0-08-100354-1.00001-6.

(14) Chevolot, Y.; Delair, T.; Laurenceau, E.; Leclercq, J.-L.; Souteyrand, E. Use of chitosan or alginate as a transfer mask in lithography and transfer methods. WO2016162638A1, October 13, 2016.

(15) Takei, S.; Oshima, A.; Ito, K.; Sugahara, K.; Kashiwakura, M.; Oyama, T. G.; Kozawa, T.; Tagawa, S.; Hanabata, M. Approach of Pullulan Derivatives to Resist Polymers for Green Lithography in Eco-Friendly Optical NEMS and MEMS; Thienpont, H., Mohr, J., Zappe, H., Nakajima, H., Eds.; Brussels, Belgium, 2014; p 913011. https://doi.org/10.1117/12.2045636.
(16) Ray, C.; Caillau, M.; Jonin, C.; Benichou, E.; Moulin, C.; Salmon, E.; Maldonado, M. E.; Gomes, A. S. L.; Monnier, V.; Laurenceau, E.; Leclercq, J.-L.; Chevolot, Y.; Delair, T.; Brevet, P.-F. Quadratic Nonlinear Optics to Assess the Morphology of Riboflavin Doped Chitosan for Eco-Friendly Lithography. *Opt. Mater.* **2018**, *80*, 30–36. https://doi.org/10.1016/j.optmat.2018.04.007.
(17) Caillau, M.; Crémillieu, P.; Laurenceau, E.; Chevolot, Y.; Leclercq, J.-L.; Alekseev, S.; Chevalier, C.; Delair, T. Fifty Nanometer Lines Patterned into Silica Using Water Developable Chitosan Bioresist and Electron Beam Lithography. *J. Vac. Sci. Technol. B Nanotechnol. Microelectron. Mater. Process. Meas. Phenom.* **2017**, *35* (6), 06GE01. https://doi.org/10.1116/1.4996870.
(18) Leclercq, J.-L.; Soppera, O.; Caillau, M.; Chevalier, C.; Crémillieu, P.; Delair, T.; Laurenceau, E.; Chevolot, Y.; Leuschel, B.; Ray, C.; Moulin, C.; Jonin, C.; Benichou, E.; Brevet, P.-F.; Yeromonahos, C. Sub-Micron Lines Patterning into Silica Using Water Developable Chitosan Bioresist Films for Eco-Friendly Positive Tone e-Beam and UV Lithography. In *Optical Microlithography XXXI*; Kye, J., Owa, S., Eds.; SPIE: San Jose, United States, 2018; p 29. https://doi.org/10.1117/12.2292312.
(19) Rinaudo, M. Chitin and Chitosan: Properties and Applications. *Prog. Polym. Sci.* **2006**, *31* (7), 603–632. https://doi.org/10.1016/j.progpolymsci.2006.06.001.
(20) Lamarque, G.; Cretenet, M.; Viton, C.; Domard, A. New Route of Deacetylation of α- and β-Chitins by Means of Freeze−Pump Out−Thaw Cycles. *Biomacromolecules* **2005**, *6*, 3, 1380–1388, https://doi.org/10.1021/bm049322b.
(21) Lamarque, G. ; Lucas, J.-M. ; Viton, C. ; Domard, A. Physicochemical Behavior of Homogeneous Series of Acetylated Chitosans in Aqueous Solution: Role of Various Structural Parameters. *Biomacromolecules* **2005**, *6*, 1, 131–142, https://doi.org/10.1021/bm0496357.
(22) Kurita, K. Chitin and Chitosan: Functional Biopolymers from Marine Crustaceans. *Mar. Biotechnol.* **2006**, *8* (3), 203–226. https://doi.org/10.1007/s10126-005-0097-5.
(23) Hirai, A.; Odani, H.; Nakajima, A. Determination of Degree of Deacetylation of Chitosan by 1H NMR Spectroscopy. *Polym. Bull.* **1991**, *26* (1), 87–94. https://doi.org/10.1007/BF00299352.
(24) Schatz, C.; Viton, C.; Delair, T.; Pichot, C.; Domard, A. Typical Physicochemical Behaviors of Chitosan in Aqueous Solution. *Biomacromolecules* **2003**, *4* (3), 641–648. https://doi.org/10.1021/bm025724c.
(25) Sekiguchi, A.; Mack, C.A.; Isono, M.; Matsuzawa, T. Measurement of parameters for simulation of deep-UV lithography using an FT-IR baking system. *Proc. SPIE* 3678, Advances in Resist Technology and Processing XVI **1999**. https://doi.org/10.1117/12.350149.
(26) Cefalas, A.C.; Sarantopoulou, E.; Gogolides, E.; Argitis, P. Absorbance and outgasing of photoresist polymeric materials for UV lithography below 193 nm including 157 nm lithography. *Microelectronic Engineering* **2000**, 53(1-4), 123-126. https://doi.org/10.1016/S0167-9317(00)00278-1.
(27) Cameron, J.F.; Chan, N.; Moore, K.; Pohlers, G. Comparison of acid-generating efficiencies in 248 and 193-nm photoresists. *Proc. SPIE* 4345, Advances in Resist Technology and Processing XVIII **2001**. https://doi.org/10.1117/12.436838.
(28) Leuschel, B.; Gwiazda, A.; Heni, W.; Diot, F.; Yu, S.-Y.; Bidaud, C.; Vonna, L.; Ponche, A.; Haidara, H.; Soppera, O. Deep-UV Photoinduced Chemical Patterning at the

Micro- and Nanoscale for Directed Self-Assembly. *Sci. Rep.* **2018**, *8* (1), 10444. https://doi.org/10.1038/s41598-018-28196-1.
(29) Dirani, A.; Roucoules, V.; Haidara, H.; Soppera, O. Plasma Polymer Tailoring of the Topography and Chemistry of Surfaces at the Nanoscale. *Langmuir* **2010**, *26* (22), 17532–17539. https://doi.org/10.1021/la1029799.
(30) Soppera, O.; Dirani, A.; Ponche, A.; Roucoules, V. Nanopatterning of Plasma Polymer Reactive Surfaces by DUV Interferometry. *Nanotechnology* **2008**, *19* (39), 395304. https://doi.org/10.1088/0957-4484/19/39/395304.
(31) Yeh, C.-C.; Liu, H.-C.; Chuang, M.-Y.; Denzer, J.; Berling, D.; Zan, H.-W.; Soppera, O. Controllable Formation of Zinc Oxide Micro- and Nanostructures via DUV Direct Patterning. *Adv. Mater. Interfaces* **2016**, *3* (19), 1600373. https://doi.org/10.1002/admi.201600373.
(32) Stehlin, F.; Wieder, F.; Spangenberg, A.; Le Meins, J.-M.; Soppera, O. Room-Temperature Preparation of Metal-Oxide Nanostructures by DUV Lithography from Metal-Oxo Clusters. *J Mater Chem C* **2014**, *2* (2), 277–285. https://doi.org/10.1039/C3TC31326C.
(33) Cennamo, N.; Arcadio, F.; Noel, L.; Zeni, L.; Soppera, O. Flexible and Ultrathin Metal-Oxide Films for Multiresonance-Based Sensors in Plastic Optical Fibers. *ACS Appl. Nano Mater.* **2021**, *4* (10), 10902–10910. https://doi.org/10.1021/acsanm.1c02345.
(34) Leceta, I.; Guerrero, P.; Ibarburu, I.; Dueñas, M. T.; de la Caba, K. Characterization and Antimicrobial Analysis of Chitosan-Based Films. *J. Food Eng.* **2013**, *116* (4), 889–899. https://doi.org/10.1016/j.jfoodeng.2013.01.022.
(35) Branca, C.; D'Angelo, G.; Crupi, C.; Khouzami, K.; Rifici, S.; Ruello, G.; Wanderlingh, U. Role of the OH and NH Vibrational Groups in Polysaccharide-Nanocomposite Interactions: A FTIR-ATR Study on Chitosan and Chitosan/Clay Films. *Polymer* **2016**, *99*, 614–622. https://doi.org/10.1016/j.polymer.2016.07.086.
(36) Corazzari, I.; Nisticò, R.; Turci, F.; Faga, M. G.; Franzoso, F.; Tabasso, S.; Magnacca, G. Advanced Physico-Chemical Characterization of Chitosan by Means of TGA Coupled on-Line with FTIR and GCMS: Thermal Degradation and Water Adsorption Capacity. *Polym. Degrad. Stab.* **2015**, *112*, 1–9. https://doi.org/10.1016/j.polymdegradstab.2014.12.006.
(37) Sionkowska, A.; Kaczmarek, H.; Wisniewski, M.; Skopinska, J.; Lazare, S.; Tokarev, V. The Influence of UV Irradiation on the Surface of Chitosan Films. *Surf. Sci.* **2006**, *600* (18), 3775–3779. https://doi.org/10.1016/j.susc.2006.01.090.
(38) Wasikiewicz, J. M.; Yoshii, F.; Nagasawa, N.; Wach, R. A.; Mitomo, H. Degradation of Chitosan and Sodium Alginate by Gamma Radiation, Sonochemical and Ultraviolet Methods. *Radiat. Phys. Chem.* **2005**, *73* (5), 287–295. https://doi.org/10.1016/j.radphyschem.2004.09.021.
(39) Yap, W. F.; Yunus, W. M. M.; Talib, Z. A.; Yusof, N. A. X-Ray Photoelectron Spectroscopy and Atomic Force Microscopy Studies on Crosslinked Chitosan Thin Film. *International Journal of the Physical Sciences*. Vol.6(11). June 2011, pp 2744–2749.
(40) Ploux, L.; Anselme, K.; Dirani, A.; Ponche, A.; Soppera, O.; Roucoules, V. Opposite Responses of Cells and Bacteria to Micro/Nanopatterned Surfaces Prepared by Pulsed Plasma Polymerization and UV-Irradiation. *Langmuir* **2009**, *25* (14), 8161–8169. https://doi.org/10.1021/la900457f.
(41) D'Almeida, M.; Attik, N.; Amalric, J.; Brunon, C.; Renaud, F.; Abouelleil, H.; Toury, B.; Grosgogeat, B. Chitosan Coating as an Antibacterial Surface for Biomedical Applications. *PLOS ONE* **2017**, *12* (12), e0189537. https://doi.org/10.1371/journal.pone.0189537.
(42) Tian, M.; Tan, H.; Li, H.; You, C. Molecular weight dependence of structure and properties of chitosan oligomers *RSC Adv.* **2015**, 5, 69445-69452. https://doi.org/10.1039/C5RA08358C.
(43) Kubota, N.; Eguchi, Y. Facile Preparation of Water-Soluble N-Acetylated Chitosan

and Molecular Weight Dependence of Its Water-Solubility. *Polymer Journal* **1997**, *29*, 123. https://doi.org/10.1295/polymj.29.123.
(44) Bergh, A. A.; Schneer, G. H. The Effect of Ionic Contaminants on Silicon Transistor Stability. *IEEE Trans. Reliab.* **1969**, *R-18* (2), 34–38. https://doi.org/10.1109/TR.1969.5216974.
(45) Gokan, H.; Esho, S.; Ohnishi, Y. J. Dry Etch Resistance of Organic Materials. *J. Electrochem. Soc.* **1983**, 130, 143. https://doi.org/10.1149/1.2119642.

Graphical Abstract